scientific reports

Check for updates

OPEN

Elucidation of anti-human melanoma and anti-aging mechanisms of compounds from green seaweed *Caulerpa racemosa*

Danar Wicaksono[1], Nurpudji Astuti Taslim[2], Vincent Lau[3], Rony Abdi Syahputra[4], Aiman Idrus Alatas[5], Purnawan Pontana Putra[6], Trina Ekawati Tallei[7], Raymond Rubianto Tjandrawinata[8], Apollinaire Tsopmo[9], Bonglee Kim[10] & Fahrul Nurkolis[11,12]✉

Human melanoma is linked with aging-related disorders, prompting interest in the development of functional foods derived from natural ingredients to mitigate its incidence. Molecules in green seaweeds such as *Caulerpa racemosa* can serve this purpose due to their anti-tumor and anti-inflammatory properties. A previous work study compounds profiling has been carried out, and in this research the molecular docking studies targeting receptors associated with melanoma (GRP78, IRE1, BRAF) and aging (mTOR, AMPK, SIRT1) identified four promising compound in an extract of *C. racemosa*. The current study aims to the mechanism of those compounds at a cellular level using the human A375 (BRAF-V600E mutation) and A375 and B16-F10 cell lines. The MTT assay was used to evaluate the potential of GSCRE compounds against A375 and B16-F10 cell lines, with comparisons made to normal HDFa cell lines. Results indicated that compound C2, also known as Caulersin, demonstrated a significantly different ΔG affinity binding score compared to the control drug Dabrafenib. GSCRE crude extract, particularly C2, showed potential in modulating mTOR, AMPK, and SIRT1 pathways and downregulating GRP78, IRE1, and BRAF signaling ($p < 0.05$). Interestingly, C2 was less effective in suppressing A375 and B16-F10 cell lines (LD_{50} C2 < LD_{50} Dabrafenib/control), with its LD_{50} value nearly matching that of the Trametinib control in B16-F10 cell lines. Consequently, GSCRE, especially C2 or Caulersin, shows promise as a new molecule for developing functional foods to combat aging and human melanoma. However, further in vivo studies and clinical trials are necessary to confirm these findings.

Keywords Anticancer, Antiaging, Green seaweed, Natural product, Melanoma, Caulerpa, Marine algae

Human melanoma, a highly aggressive form of skin cancer, has seen a significant increase in incidence worldwide[1,2]. According to recent statistics, approximately 132,000 new cases of melanoma are diagnosed

[1]Alumnus Department of Dermatology and Venereology, Faculty of Medicine, Public Health, and Nursing, Universitas Gadjah Mada, Yogyakarta, Indonesia. [2]Division of Clinical Nutrition, Department of Nutrition, Faculty of Medicine, Hasanuddin University, Makassar 90245, Indonesia. [3]Faculty of Medicine, Public Health, and Nursing, Universitas Gadjah Mada, Yogyakarta 55281, Indonesia. [4]Department of Pharmacology, Faculty of Pharmacy, Universitas Sumatera Utara, Medan 20155, Indonesia. [5]Program of Clinical Microbiology Residency, Faculty of Medicine, Universitas Indonesia, Jakarta, Indonesia. [6]Department of Pharmaceutical Chemistry, Faculty of Pharmacy, Universitas Andalas, Padang 25163, Indonesia. [7]Department of Biology, Faculty of Mathematics and Natural Sciences, Sam Ratulangi University, Manado 95115, Indonesia. [8]Center for Pharmaceutical and Nutraceutical Research and Policy, Faculty of Biotechnology, Atma Jaya Catholic University of Indonesia, Jakarta 12930, Indonesia. [9]Food Science and Nutrition Program, Department of Chemistry, Carleton University, 1125 Colonel by Drive, Ottawa, ON K1S 5B6, Canada. [10]Department of Pathology, College of Korean Medicine, Kyung Hee University, Kyungheedae-Ro 26, Dong-Daemun-Gu, Seoul 05254, South Korea. [11]Department of Biological Sciences, Faculty of Sciences and Technology, State Islamic University of Sunan Kalijaga (UIN Sunan Kalijaga), Yogyakarta 55281, Indonesia. [12]Medical Research Center of Indonesia (MERCIE), Surabaya 60281, Indonesia. ✉email: fahrul.nurkolis.mail@gmail.com

No	Observed compounds	Molecular formula	Molecular weight (g/mol)	Substance ID (PubChem)
C1	Caulerpin	$C_{24}H_{18}N_2O_4$	398.4	5,326,018
C2	Caulersin	$C_{21}H_{14}N_2O_3$	342.3	10,593,388
C3	Caulerpenyne	$C_{21}H_{26}O_6$	374.4	5,311,436
C4	Racemosin	$C_{16}H_{16}O_5$	288.29	155,148

Table 1. The metabolites that were detected in Green Seaweed *C. Racemosa*extract (GSCRE) using HPLC-ESI-HRMS/MS analysis[17].

	Pa level*		Analysis of toxicity computation**		Drug likeness***		
No	Kinase inhibitor	Antineoplastic	LD_{50} prediction (mg/kg)	Class of toxicity	Lipinski	Pfizer	GSK
C1	0.727	0.711	1,760	4	Accepted	Accepted	Rejected
C2	0.815	0.711	3.000	5	Accepted	Rejected	Rejected
C3	0.558	0.810	500	4	Accepted	Accepted	Accepted
C4	0.434	0.796	1,050	4	Accepted	Rejected	Accepted

Table 2. The evaluation of GSCRE as a potential anticancer agent was performed by assessing its structure-activity relationship (SAR) predictions, Pa level, toxicity computational analysis, and drug likeness[17]. *Way2Drug; **Protox; ***ADMET.

globally each year, with a notable rise in prevalence particularly in countries with high ultraviolet exposure[2]. In the United States alone, an estimated 100,640 new melanomas are expected to be diagnosed in 2024, with approximately 8,290 fatalities attributed to the disease[3]. This growing burden of melanoma highlights the critical need for novel therapeutic approaches.

Current treatment modalities for melanoma include surgical resection, chemotherapy, targeted therapies (such as BRAF and MEK inhibitors), and immunotherapies (like checkpoint inhibitors targeting CTLA-4 and PD-1)[4–7]. While these treatments have improved patient outcomes, they are often accompanied by significant side effects, high costs, and the development of resistance[4–7].These challenges necessitate the exploration of alternative therapies[8], including natural products with potential anticancer properties[9].

Marine algae, particularly green algae, have shown promise as sources of bioactive compounds with diverse therapeutic potentials[10]. Green algae have been studied for their anticancer, antioxidant, and anti-inflammatory properties[10–12]. *Caulerpa racemosa*, a species of green seaweed, has demonstrated potential anticancer activity in various studies. For example, polysaccharides from *C. racemosa*exhibited significant antitumor activity against hepatocellular carcinoma cell lines, showing inhibition rates of 59.5–83.8% in experimental models[13,14]. Despite these promising results, the specific efficacy of *C. racemosa* against melanoma has not been extensively investigated.

Previous research on the anticancer potential of *C. racemosa* has primarily focused on other cancer types, such as colorectal cancer and hepatoma. For instance, studies have identified compounds like caulerpin from *C. racemosa*that showed binding affinity in molecular docking studies but with limited total binding energy, indicating the need for further optimization[13,15]. Additionally, sulfated polysaccharides from *C. racemosa*have been explored for their antioxidant and anticancer activities, demonstrating potential as functional food ingredients and therapeutic agents[16]. However, a significant gap remains in understanding the specific molecular mechanisms and efficacy of *C. racemosa* against melanoma.

This study aims to address this gap by investigating the anti-melanoma and anti-aging potential of *C. racemosa* extract (GSCRE) and its compounds through comprehensive in vitro and in silico analyses. The study will conduct molecular docking to identify bioactive compounds within GSCRE that interact with key receptors involved in melanoma (GRP78, IRE1, BRAF) and aging (mTOR, AMPK, SIRT1). These findings will be complemented by ex vivo cellular assays on human melanoma cell lines (A375 and B16-F10) to evaluate the cytotoxic effects of GSCRE compounds. By integrating these approaches, the study aims to identify novel molecules from GSCRE with therapeutic potential against melanoma and aging-related diseases, providing a basis for future in vivo studies and clinical trials.

Results

In a previous study published in the Marine Drugs journal, the authors characterized the metabolites and specific compounds of GSCRE[17]. The results of this characterization are presented in Table 1 of the study. Additionally, an in silico or computational study was conducted to explore structure-activity relationship (SAR) predictions, Pa values, toxicity computational analysis, and drug-likeness.

The data from these analyses are presented in Table 2 of the study. The study found that the four compounds from GSCRE exhibited a Probability Activity (Pa) Score greater than 0.40 as kinase inhibitors and antineoplastic agents, as shown in Table 2. Furthermore, the cytotoxicity prediction values placed these compounds in toxicity classes 4 and 5 (greater than 3), indicating their potential for development as functional food candidates.

After the SAR prediction presented in Table 2, the compounds identified in GSCRE underwent molecular docking studies against six selected receptors: GRP78, IRE1, and BRAF, which are related to melanoma, and AMPK, MTOR, and SIRT1, which are associated with aging. The differences in the ΔG affinity binding scores between the GSCRE compounds and the control drugs are shown in Table 3. Control drugs Dabrafenib and Trametinib were used as controls. Table 3 reveals that compound C2, or Caulersin, exhibited a more potent/inferior overall ΔG affinity binding score compared to the control drug Dabrafenib, though its score was still slightly below that of Trametinib. Notably, for the SIRT1 receptor, the ΔG values of C2 or Caulersin were superior/inferior to both control drugs, indicating a distinctive binding affinity profile (Table 3).

The Table 4 presents a visual depiction of the interactions between the identified compounds C1 and C2 of GSCRE and amino acids, as well as the control drugs targeting specific proteins/receptors. Table S1 contains comprehensive information on the specific interactions of all compounds. The efficacy of these substances is contingent upon the quantity and potency of the interactions with amino acids, which impede the transmission of signals to the receptor/protein. The binding affinity of these amino acids is correlated with their ability to flexibly utilize these compounds. An enhanced comprehension of a compound's affinity can be achieved by examining the potency of binding interactions, specifically through hydrogen bonds. The majority of the compounds in GSCRE establish hydrogen bonds with amino acids that are engaged in the mTOR/AMPK/SIRT1 and GRP78/IRE1/BRAF signaling pathways. This suggests that there are differences in the levels of docking activity among the substances, which can be linked to their chemical structure and functional properties. The results of molecular docking analysis demonstrated that Caulersin (C2) possesses a strong affinity for specific receptors that have been carefully chosen. This finding emphasizes the potential of Caulersin (C2) as a bioactive compound in the treatment of cancer pathways and premature aging.

The molecular dynamics simulation of BRAF and mTOR proteins focused on chain D, as Caulersin, during docking, interacted specifically with this chain. In the molecular dynamics simulation of BRAF (Fig. 1A, the RMSD fluctuated within a range of 1 to 2.4 nm. Initially, from 0 to 10 ns, the movement of the molecule remained around 1 nm. After 12 ns, there was a jump from 1 nm to 2 nm, lasting until 20 ns. Following this, the RMSD decreased, reaching 1 nm by 20 ns, with fluctuations ranging between 0.8 and 1.25 nm until 60 ns. After 60 ns, fluctuations between 1 and 2.25 nm were observed. The molecular movement stabilized between 63 ns and 75 ns, maintaining a steady value around 2.25 nm from 75 ns to 90 ns. Figure 1A of BRAF shows that the RMSD of the protein and ligand fluctuated between 0.5 nm and 2.5 nm. In contrast, the mTOR protein (Fig. 1B), under the same conditions, exhibited more stable molecular behavior, with RMSD values ranging from 0.1 to 0.3 nm. A significant increase in RMSD, reaching 0.5 nm, was observed between 32 ns and 35 ns. Overall, based on RMSD values, Caulersin exhibited greater stability when simulated with the mTOR protein compared to BRAF.

In the BRAF protein (Fig. 2A), residues Thr193 (0.0744 nm), Leu172 (0.0865 nm), and Cys173 (0.0872 nm) exhibit low RMSF values, indicating that these regions are more stable, likely due to direct interactions with cyclic nucleotides. Thr193 is especially critical as it interacts with the guanine ring of cGMP, acting as an anchor for both the cyclic phosphate and guanine portions, which stabilizes the cGMP molecule in its syn conformation. Mutations at this site could potentially affect the selective binding of cGMP by protein kinase G (PKG) over cAMP. Additionally, Leu172 and Cys173 form a unique binding site for guanine in cGMP, further enhancing the protein's affinity through a cis-peptide bond. These residues create a precise docking point for the purine ring, contributing to the specificity of the interaction. On the other hand, the highest fluctuations are observed for Ser92 (0.5411 nm) and Asn121 (0.1984 nm), which indicates these regions are more flexible during the simulation. In the mTOR protein (Fig. 2B), the most prominent fluctuations occur at residues Gly204 (0.7838 nm) and Gly263 (0.4653 nm), suggesting that these regions are particularly flexible due to the influence of Caulersin. These elevated RMSF values highlight the dynamic movement of these residues during the simulation, reflecting the increased flexibility in response to Caulersin binding.

The solvent accessible surface area (SASA) data for BRAF and mTOR proteins reveal key insights into their behavior during the 100 ns molecular dynamics simulation. For BRAF (Fig. 3A), the surface area fluctuates widely between 70 nm^2 and 78 nm^2, especially in the early stages of the simulation, indicating significant changes in how much of the protein is exposed to the solvent. This suggests that BRAF undergoes considerable conformational changes, likely reflecting a flexible structure. In contrast, mTOR shows more moderate fluctuations, ranging between 135 nm^2 and 154 nm^2, with a noticeable drop in SASA between 10 and 50 ns, potentially indicating a compacting phase. After 50 ns, mTORs surface area stabilizes, suggesting that it reaches a more consistent

	Melanoma-related receptors proteins			Aging-related receptor proteins			
Compound and controls as ligands	GRP78	IRE1	BRAF	AMPK	mTOR	SIRT1	Overall
Dabrafenib	-9.3	-8.7	-9.9	-9.1	-11.2	-8.5	-56.7
Trametinib	-9.2	-10.4	-11.3	-9.9	-12.4	-8.7	-61.9
C1	-8.4	-7.6	-9.4	-9.0	-8.7	-9.0	-52.1
C2	-8.9	-9.5	-9.3	-9.3	-10.2	-10.5	-57.7
C3	-8.1	-6.9	-7.8	-7.9	-7.9	-9.6	-48.2
C4	-8.7	-7.5	-8.3	-8.0	-8.1	-8.5	-49.1

Table 3. The difference of ΔG values from the molecular docking analysis between GSCRE compounds and the controls.

Proteins	C1	C2
GRP78	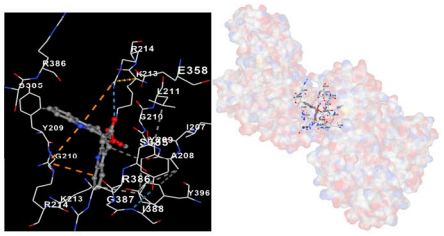	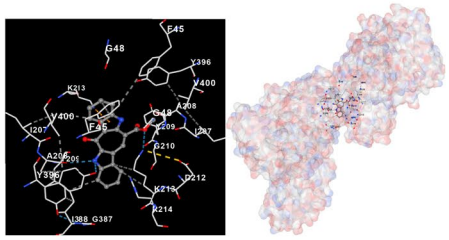
IRE1	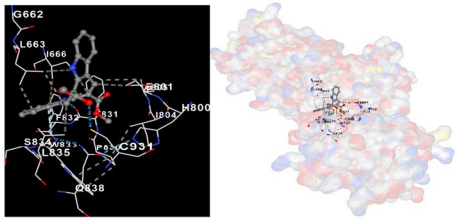	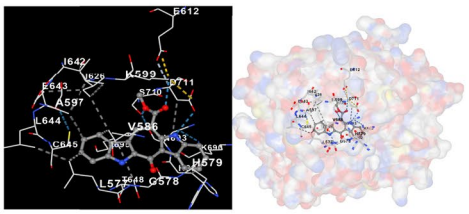
BRAF	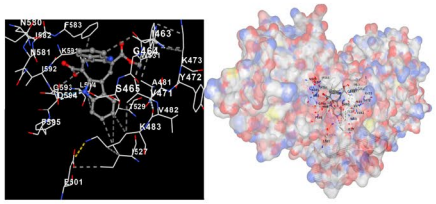	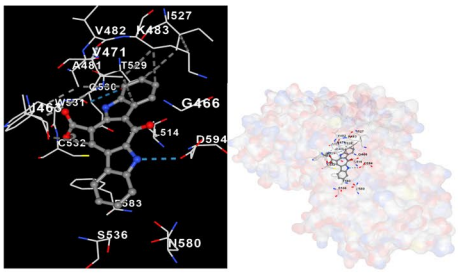
AMPK	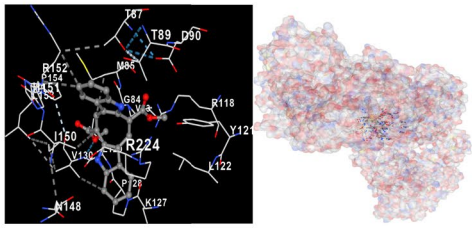	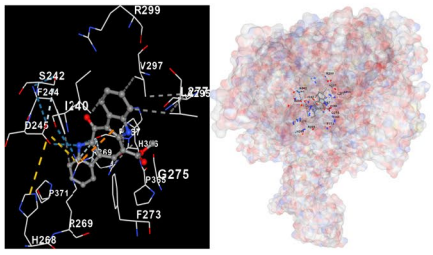
mTOR	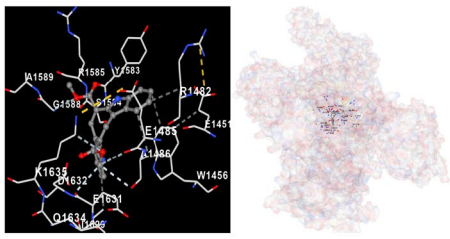	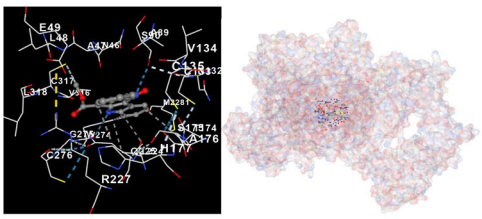
SIRT1	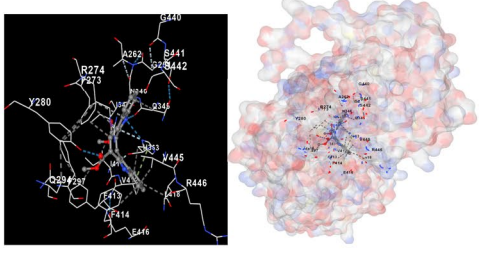	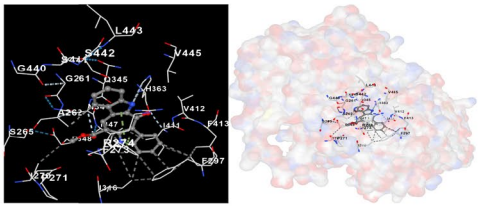

Table 4. Graphical depiction of the interaction between amino acids and the compounds identified from GSCRE with specific receptor proteins.

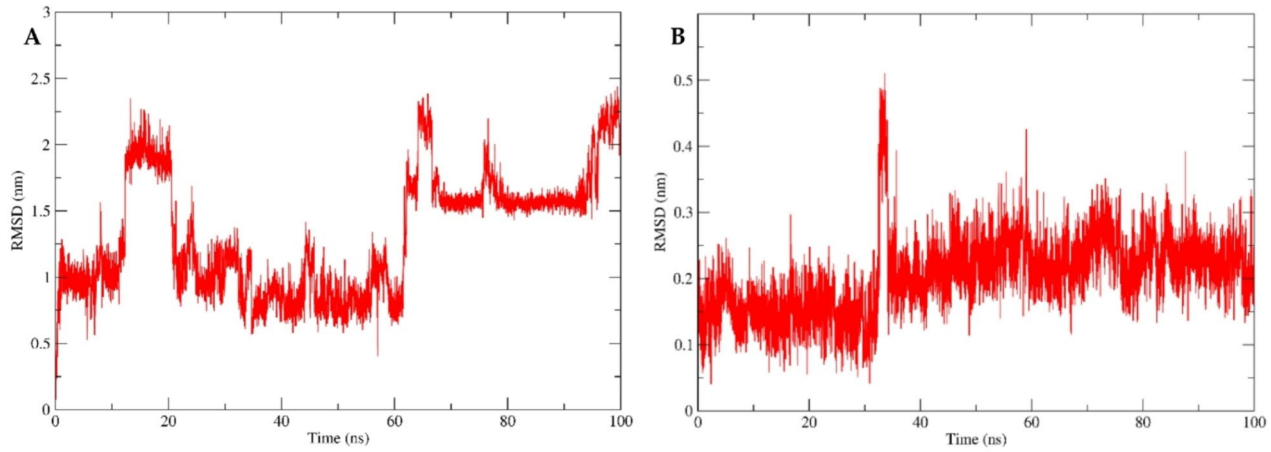

Fig. 1. (**A**) RMSD graph of the BRAF protein. (**B**) RMSD graph of the mTOR protein. The interaction dynamics between Caulersin and the BRAF and mTOR proteins are represented by RMSD values, which reflect the stability of the binding between Caulersin and the BRAF and mTOR proteins.

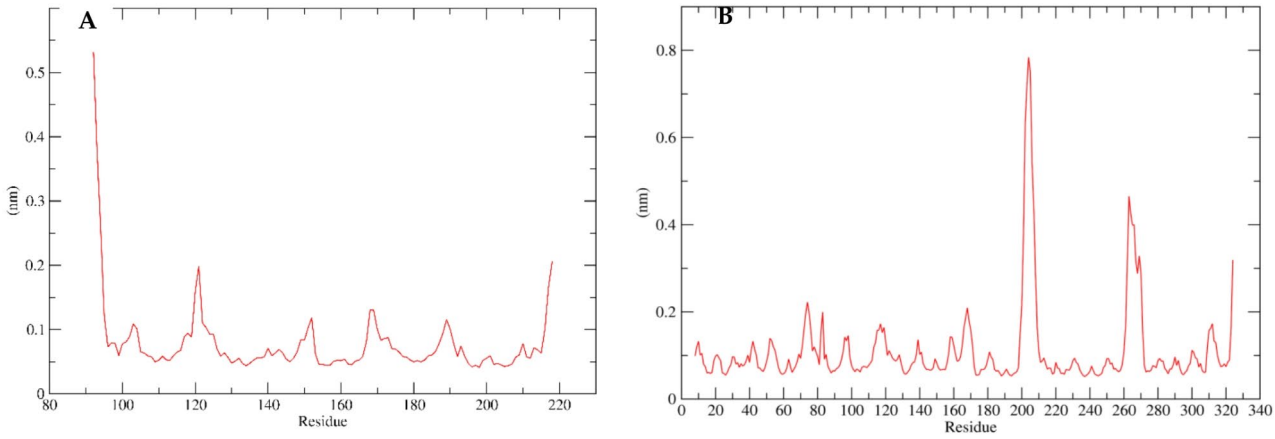

Fig. 2. Root Mean Square Fluctuation (RMSF) of BRAF and mTOR proteins. (**A**) RMSF graph of the BRAF protein. (**B**) RMSF graph of the mTOR protein. The interaction dynamics between Caulersin and the BRAF and mTOR proteins are captured by the RMSF values, which reflect the fluctuation of each residue due to Caulersin's binding.

and stable structure compared to BRAF (Fig. 3B). Overall, while BRAF demonstrates greater flexibility, mTOR appears to adopt a more stable conformation during the simulation.

In this simulation (Fig. 4), with Caulersin as the ligand, BRAF maintains structural stability with a relatively constant Radius of Gyration (Rg) around 1.4 nm, indicating that the presence of Caulersin does not significantly affect its conformation (Fig. 4A). In contrast, mTOR exhibits greater fluctuations, with Rg values ranging between 1.825 nm and 1.90 nm, suggesting increased flexibility and dynamic structural changes (Fig. 4B). After an initial compaction around 20 ns, mTOR continues to undergo conformational adjustments, indicating that it may be more responsive to Caulersin. This difference in Rg values highlights the distinct interactions of these proteins with the ligand throughout the simulation.

The molecular mechanics-generalized born surface area (MM-GBSA) analysis in Fig. 5 reveals that Caulersin has a stronger binding affinity to mTOR than BRAF, as reflected by the more negative ΔG of -32.06 kcal/mol for mTOR, compared to -17.79 kcal/mol for BRAF in Fig. 5. The GGAS (gas phase energy) component, which includes van der Waals and electrostatic interactions, plays a significant role in both proteins, but is much more pronounced in mTOR (-49.21 kcal/mol) than in BRAF (-23.17 kcal/mol), indicating stronger non-covalent interactions with mTOR. On the other hand, the GSOLV (solvation energy) component, which represents the desolvation penalty, is higher for mTOR (17.15 kcal/mol) than BRAF (5.38 kcal/mol), reflecting the greater energy cost to desolvate mTOR. Despite this higher penalty, mTOR still maintains a stronger overall binding interaction with Caulersin due to the significantly greater GGAS contribution, highlighting the stability and strength of the ligand-protein interaction.

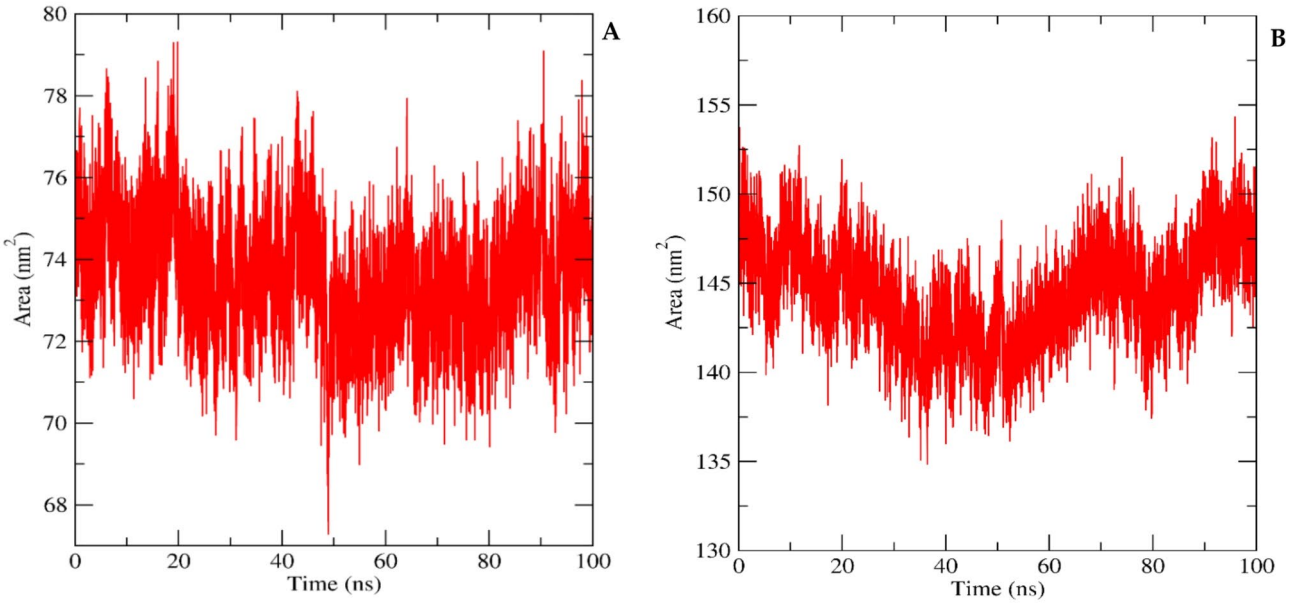

Fig. 3. Solvent Accessible Surface Area (SASA) Analysis. (**A**) SASA profile of the BRAF protein. (**B**) SASA profile of the mTOR protein. These profiles represent the solvent-accessible surface area of the proteins, indicating the extent to which the protein surface is exposed to solvent molecules during the molecular dynamics simulation. Higher SASA values suggest greater solvent exposure, while lower values indicate more compact or buried regions within the protein.

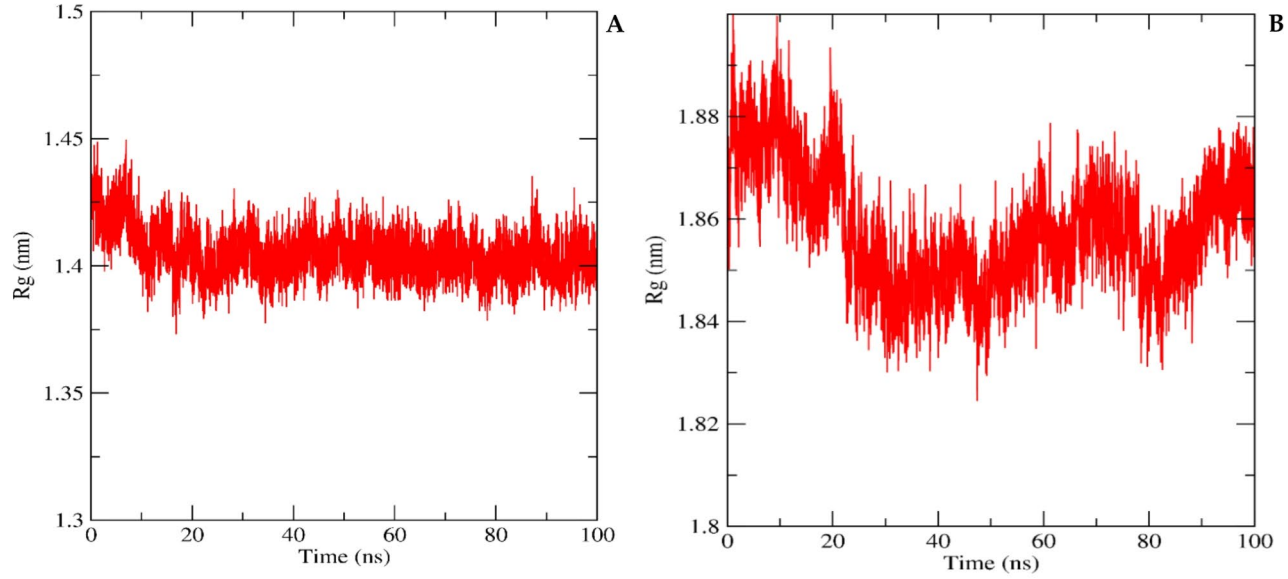

Fig. 4. Radius of Gyration of (**A**). BRAF Protein with Caulersin and (**B**). mTOR Protein with Caulersin. The radius of gyration (Rg) refers to how atoms in a protein are spread out around its central axis. It measures the average distance between the center of rotation and the point where energy transfer is most effective.

The molecular dynamics simulations reveal that Caulersin interacts more stably and favorably with the mTOR protein compared to BRAF. The RMSD and RMSF analyses indicate that mTOR shows greater structural stability, with fewer fluctuations and more consistent behavior, whereas BRAF exhibits more dynamic changes and higher flexibility. The SASA analysis further supports this, showing that mTOR adopts a more compact and stable structure during the simulation, while BRAF experiences larger conformational shifts. The radius of gyration analysis reinforces these findings, as BRAF remains stable while mTOR undergoes more conformational

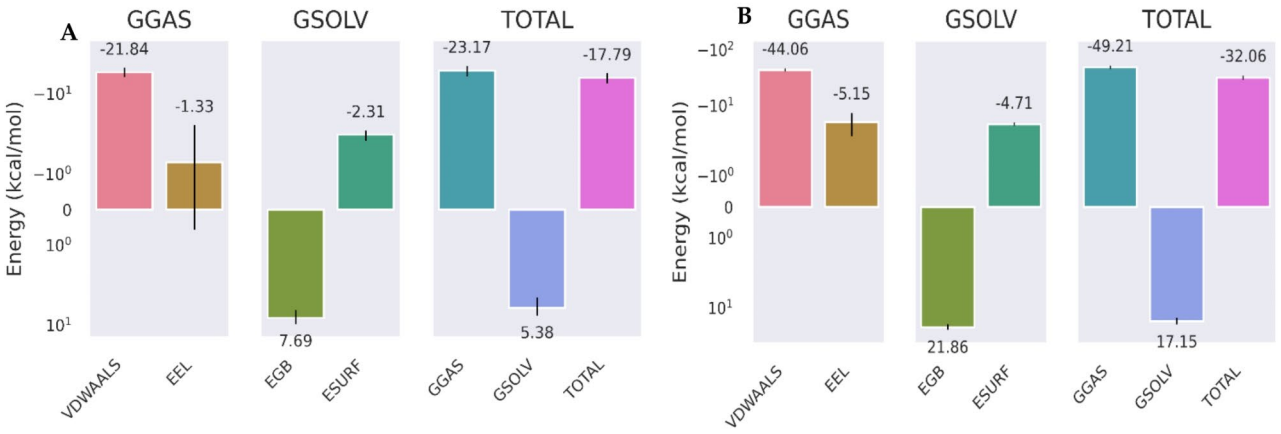

Fig. 5. The free energy values calculated using the MMGBSA approach represent the ΔG (binding free energy) between Caulersin and the BRAF protein. The binding free energy for Caulersin with BRAF is -17.79 kcal/mol (Fig. 5A), while in Fig. 5B, the ΔG value between Caulersin and the second protein is -32.06 kcal/mol. (**A**) BRAF (**B**) mTOR.

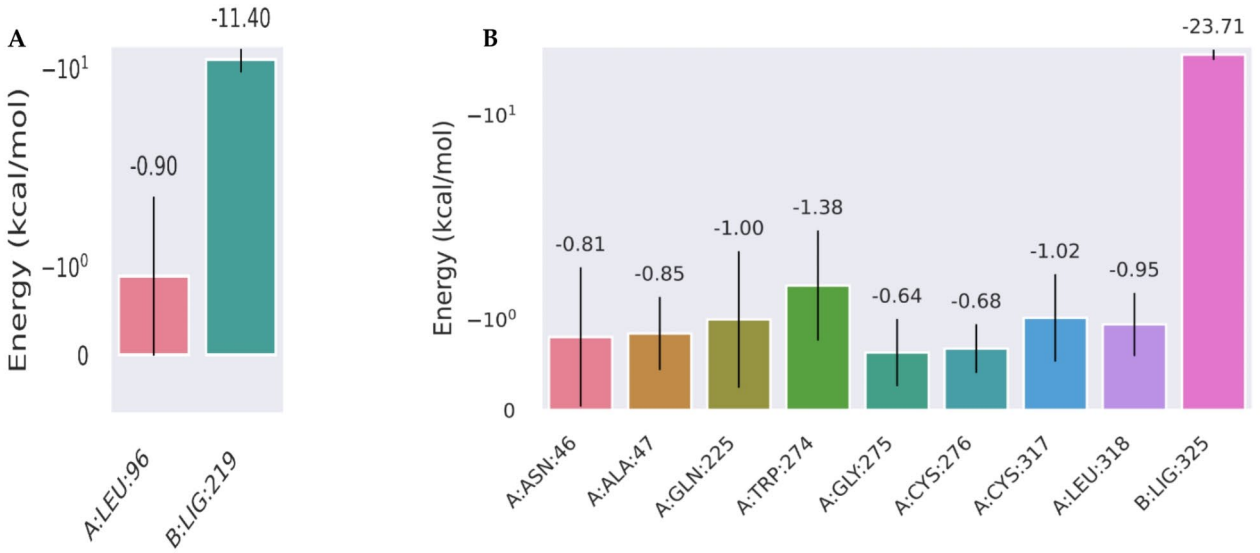

Fig. 6. (**A**) Decomposition energy illustrating the effect of Caulersin on the BRAF protein. (**B**) Decomposition energy illustrating the effect of Caulersin on the mTOR protein. This analysis shows how Caulersin impacts specific amino acid residues in terms of energy.

adjustments in response to Caulersin binding. Finally, the MM-GBSA results demonstrate a stronger binding affinity between Caulersin and mTOR, driven by more favorable van der Waals and electrostatic interactions, highlighting the higher stability and strength of the ligand-protein interaction with mTOR. Overall, Caulersin forms a more energetically favorable and stable complex with mTOR compared to BRAF.

Figure 6 presents the decomposition energy analysis of Caulersin interaction with the BRAF and mTOR proteins. In Fig. 6A, the graph shows how Caulersin affects two specific residues in the BRAF protein such as Leu 96 and LIG 219 (Caulersin). The energy contributions from these residues indicate that LIG 219 (Caulersin) has a much stronger binding energy − 11.40 kcal/mol, while Leu 96 contributes less than − 0.90 kcal/mol. In Fig. 6B, the Caulersin influences several residues in the mTOR protein, with the strongest interaction observed at LIG 325 (Caulersin) with energy − 23.71 kcal/mol. Other residues, such as Gly 274, Asn 46, and Trp 274, contribute moderately to the binding energy. The decomposition energy values show that Caulersin significantly impacts specific residues within mTOR, particularly Caulersin, suggesting a strong interaction with this site.

The mTOR/AMPK/SIRT1 signaling pathway is crucial for understanding the anti-aging potential of a compound, while the GRP78/IRE1/BRAF pathway is significant in studying anti-cancer compounds for melanoma. In this study, in silico molecular docking (as shown in Tables 3 and 4) demonstrated that the

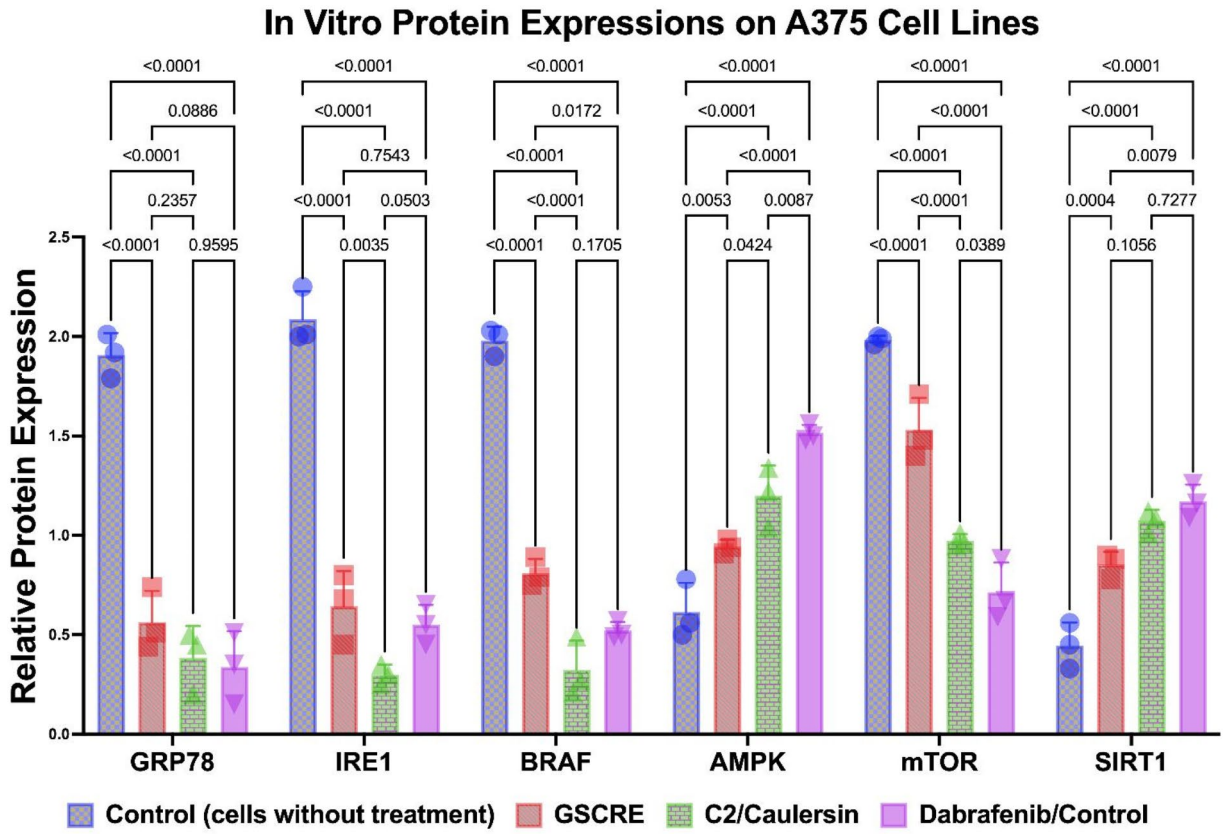

Fig. 7. Modulation of mTOR/AMPK/SIRT1 and GRP78/IRE1/BRAF by GSCRE and C2/Caulersin.

Samples	A375 cell lines	B16-F10 cell lines	Normal cell lines (HDFa)
Dabrafenib	450.3500	235.0059	600.0354
Trametinib	105.5000	94.3444	345.6600
GSCRE	325.0024	180.3555	1,200.3044
C1	306.3444	220.8770	1,000.5600
C2	185.4500	118.4600	987.8955

Table 5. LD_{50} values (μg/mL) exhibited by GSCRE on A375 and B16-F10 cell lines, and normal cell lines.

compounds in GSCRE, particularly C2 (Caulersin), have notable biological activity against the mTOR/AMPK/SIRT1 and GRP78/IRE1/BRAF protein receptors. These findings were further investigated at the cellular level through in vitro or ex vivo studies on A375 cells, with data presented in Fig. 7. The results indicate that GSCRE and C2 play a role in modulating the mTOR/AMPK/SIRT1 pathways and downregulating GRP78/IRE1/BRAF signaling compared to the control (cells without treatment; $p < 0.05$). Notably, C2 showed activity equivalent to the control drug Dabrafenib ($p > 0.05$) in the upregulation of AMPK/SIRT1, coupled with the suppression of mTOR protein. Furthermore, when compared to Dabrafenib, C2 did not significantly differ ($p > 0.05$) in suppressing the GRP78/IRE1/BRAF protein receptors, indicating similar activity between C2 and Dabrafenib. These findings underscore the potential of GSCRE and C2 in their roles as anti-aging and anti-cancer agents for melanoma at both molecular and cellular levels. Consequently, GSCRE and C2 have advanced to confirmation tests for melanoma cancer cells ex vivo/in vitro.

After assessing the modulation of the mTOR/AMPK/SIRT1 and GRP78/IRE1/BRAF pathways (as shown in Fig. 7), in vitro tests were conducted to evaluate the efficacy of GSCRE and its compounds in suppressing A375 cell lines with the BRAF-V600E mutation and B16-F10 cell lines. This evaluation included comparisons with normal HDFa cell lines (Primary Dermal Fibroblast; Normal, Human, Adult), with the 50% Lethal Dose (LD_{50}) data presented in Table 5. The data indicates that C2 is less effective in suppressing A375 and B16-F10 cell lines (LD_{50} C2 < LD_{50} Dabrafenib/control). However, the LD_{50} value of C2 is nearly equivalent to that of Trametinib in suppressing B16-F10 cell lines. Moreover, GSCRE and C2 exhibit relatively safe LD_{50} values in normal HDFa cells ($LD_{50} > 600$ μg/mL). This suggests that C2 has good potential in suppressing both the BRAF-

V600E mutation (A375) and the B16-F10 melanoma cancer cell lines, while maintaining moderate safety in normal cells. Therefore, C2 shows promise as a new molecule for the development of functional foods aimed at treating melanoma and other aging-related disorders.

Discussion

Caulerpa racemosa, a type of green seaweed, has demonstrated promising potential as an anti-cancer agent, particularly against non-small cell lung cancer (NSCLC). Research by Lau (2024) highlights Caulersin (C2), a compound found in the extract, as a potent inhibitor of non-small cell lung cancer[17]. Additionally, *C. racemosa* contains phenolic compounds that act as antioxidants[18], which could be beneficial in combating oxidative stress associated with melanoma.

Our study conducted molecular docking analyses on metabolite components of GSCRE to evaluate their potential as therapeutic agents. The targeted receptors included GRP78, IRE1, and BRAF, which are related to melanoma, as well as AMPK, mTOR, and SIRT1, which are associated with aging. Dabrafenib and trametinib, known for their significant efficacy in treating melanoma, particularly in patients with BRAF V600 mutations, served as control drugs. Our docking results reveal that compound C2, Caulersin, exhibited a ΔG affinity binding score more potent than Dabrafenib, although its score was still slightly below that of Trametinib. Notably, for the SIRT1 receptor, the ΔG values of Caulersin were superior to both control drugs, indicating a distinctive binding affinity profile. Our in vitro data showed that Caulersin had activity equivalent to Dabrafenib in the upregulation of AMPK/SIRT1, coupled with the suppression of mTOR protein. Furthermore, compared to Dabrafenib, Caulersin did not significantly differ ($p > 0.05$) in suppressing the GRP78/IRE1/BRAF protein receptors, indicating similar activity between Caulersin and Dabrafenib.

BRAF mutations play a significant role in melanoma, with the BRAF V600E mutation being the most common, present in approximately 50% of cutaneous melanomas[19]. This mutation is associated with various clinical implications, including a younger age of onset and shortened survival in high-risk melanoma cases[20]. Additionally, mutations in BRAF codons 594 and 596 have been identified as potential good prognostic factors for melanoma[21]. The prevalence of BRAF mutations in primary melanoma ranges from 33 to 47%, increasing to 41–55% in metastatic melanoma, with recurrent melanoma showing an even higher frequency of BRAF mutations[22]. BRAF mutations, particularly BRAF V600E, are known to activate the MAP kinase signaling pathway, leading to increased melanoma cell proliferation[23]. The presence of BRAF mutations has been associated with better responses to BRAF-inhibiting drugs like vemurafenib compared to traditional chemotherapy[24]. Furthermore, BRAF mutations have been identified as predictive and prognostic biomarkers for cutaneous melanoma[25]. The BRAF V600E mutation has been linked to a worse prognosis in cutaneous melanoma[26]. In the context of treatment, BRAF inhibitors, often used in combination with MEK inhibitors, have shown promise in treating advanced BRAF-mutant melanoma[27]. Additionally, immunohistochemical staining for BRAF V600E has been utilized to predict the prognosis of patients with cutaneous melanoma[25]. The mutational status of BRAF has been explored in various contexts, including its role in resistance to vemurafenib and its association with interleukin-10 production in melanoma cells[28]. BRAF mutations, particularly the BRAF V600E mutation, are prevalent in melanoma and have significant implications for diagnosis, prognosis, and treatment outcomes in patients with this type of cancer. Targeting BRAF protein in BRAF mutant melanoma is crucial for developing targeted therapies and improving patient care.

Melanoma, a type of skin cancer, has been extensively studied in relation to the glucose-regulated protein 78 (GRP78) pathway. GRP78, also known as BiP, plays a crucial role in regulating the unfolded protein response (UPR) pathway, essential for cellular homeostasis and survival. Several studies have highlighted the significance of GRP78 in melanoma progression and treatment. Research has shown that targeting GRP78 can have therapeutic implications in melanoma treatment. For example, the inhibition of the MEK/ERK pathway sensitizes melanoma cells to endoplasmic reticulum (ER) stress-induced apoptosis by downregulating GRP78 expression[29]. Additionally, antibodies targeting the C-terminal region of GRP78 interfere with signaling cascades that promote cell growth and proliferation, offering potential therapeutic applications[30]. Furthermore, the upregulation of GRP78 is associated with melanoma malignancy and progression[31]. Studies have also demonstrated that GRP78 is overexpressed in cancer cells and correlates with the progression of melanoma[32]. Moreover, the Cripto and GRP78 complex enhances tumor growth by inhibiting TGF-β signaling[33]. In melanoma, the UPR pathway, involving key components like IRE1, XBP1, and ATF6, interacts with GRP78 to regulate cell survival and apoptosis[34]. The contribution of IRE1α to the increase in GRP78 mRNA levels has been highlighted in melanoma cells[35]. Additionally, the interaction of GRP78 with other proteins and pathways, such as the MEK/ERK pathway, influences melanoma cell fate and response to therapies[36,37].

The IRE1 pathway is a critical player in melanoma progression, regulating cell survival and apoptosis mechanisms. In melanoma cells, IRE1 activity is sustained through the MEK/ERK pathway, countering PERK-mediated apoptosis and promoting cell survival[38,39]. The IRE1-XBP1 pathway is hyperactivated in melanoma, resulting in increased XBP1s expression in tumor specimens compared to normal tissues[40]. This pathway has been linked to cell proliferation in various cancers, including melanoma[41]. Activation of IRE1 or XBP1s in response to IL-6 can enhance JAK/STAT signaling, promoting tumor cell proliferation in melanoma[42]. Additionally, the IRE1-XBP-1 axis is involved in downregulating c-Myc and activating NK cells, providing protection against melanoma[43]. Research indicates that the UPR, particularly the IRE1 pathway, is a key factor in melanoma progression and metastasis[44]. In melanoma cells, the IRE1-XBP1 pathway can be activated under ER stress conditions, leading to cell death mechanisms[45]. Furthermore, the UPR can induce autophagy in response to ER stress in melanoma cells, contributing to chemoresistance[46]. Interestingly, simultaneous inhibition of BRAF and PERK in melanoma cells has been shown to sensitize them to ER stress-induced apoptosis, suggesting a potential strategy to overcome chemoresistance[47].

Research has shown that GSCRE exhibits antioxidant activity[18,48,49], which is a key factor in combating aging processes by reducing oxidative stress. Studies have also highlighted the anti-inflammatory properties of GSCRE[50,51], which can help in preventing inflammation-associated aging. Moreover, GSCRE has been found to have anti-obesity effects[14,52], which is significant as obesity is a risk factor for accelerated aging. The extract has also shown potential in regulating lipid profiles[53], which can contribute to overall health and potentially slow down the aging process. Furthermore, GSCRE has demonstrated antimicrobial activity[54,55], which is important for maintaining skin health and preventing age-related skin issues. Studies have also indicated that the extract may have antiviral properties[56], which could be beneficial in protecting against viral infections that can impact overall health and aging. Overall, the diverse bioactive compounds present in GSCRE, such as antioxidants, anti-inflammatory agents, and antimicrobial components, collectively contribute to its potential as an anti-aging agent. By targeting multiple pathways associated with aging, GSCRE shows promise in promoting healthy aging and addressing age-related concerns.

The mTOR/AMPK/SIRT1 pathway is a critical regulator of aging, influencing processes such as autophagy, oxidative stress response, and cellular metabolism. The study by Hayes (2023) investigates the potential of Coffee Silverskin (CS) phytocompounds as a novel anti-aging functional food. The research involves profiling metabolites and phytochemicals present in CS, evaluating antioxidant properties, and exploring potential anti-aging effects through molecular docking simulation and in vitro modulation of the mTOR/AMPK/SIRT1 pathway[57]. The findings suggest that CS may possess anti-aging properties mediated through the mTOR/AMPK/SIRT1 pathway, highlighting a promising area for further research in the field of anti-aging interventions.

Research has demonstrated that mTOR signaling plays a critical role in aging and age-related diseases, impacting processes like cardiac aging, heart failure, and age-related diseases[58]. Moreover, deregulation of the mTOR signaling pathway has been associated with multiple age-related diseases, including cancer, neurodegeneration, and autoimmunity[59]. The mTOR pathway is widely recognized as one of the most significant pathways involved in the aging process, with the inhibition of this pathway being a potential therapeutic target to delay aging and age-related pathologies[60]. The mTOR pathway has been linked to cellular senescence, organismal aging, and hyper-functional signaling pathways, such as mTOR, which are associated with aging[61]. Studies have shown that inhibiting the mTOR pathways through various methods can extend lifespan[62].

Activation of AMPK has been demonstrated to protect cells from senescence induced by oxidative stress through mechanisms involving restoration of autophagic flux and elevation of intracellular NAD^+ levels[63]. Furthermore, AMPK activation has been associated with the inhibition of myeloid-derived suppressor cells, which contribute to aging through NF-κB and mTOR-mediated signaling pathways[64]. Additionally, AMPK signaling has been shown to inhibit myofibroblast differentiation, impacting age-related tissue fibrosis and degeneration[65]. Research has highlighted the interaction between AMPK and other pathways in aging. For example, miR-146a has been found to hinder the anti-aging effect of AMPK by suppressing NAMPT and deactivating NAD^+/SIRT1, thus affecting the aging process[66]. Moreover, the AMPK/SIRT1 pathway has been demonstrated to enhance cellular longevity, mitochondrial function, autophagy, and reduce oxidative stress and apoptosis, all of which are crucial in the aging process[67]. The AMPK pathway has been implicated in various age-related conditions. For instance, dysregulated autophagy mediated by AMPK signaling pathways contributes to sarcopenic obesity and its complications, underscoring the role of AMPK in age-related metabolic disorders[68]. Additionally, AMPK activation has been shown to alleviate D-galactose-induced cardiomyocyte senescence by promoting autophagy through the SIRT1/AMPK/mTOR pathway[69].

The SIRT1 pathway is known to play a crucial role in aging-related processes by regulating various biological pathways. SIRT1, a NAD^+-dependent deacetylase, is involved in cellular senescence, oxidative stress, inflammation, DNA repair, apoptosis, and metabolic homeostasis[70–76]. Studies have shown that SIRT1 interacts with key molecules and signaling pathways associated with aging, such as p53, NF-κB, Nrf2, and AMPK, to exert its anti-aging effects[77–82]. Activation of SIRT1 has been linked to the suppression of cellular senescence, inflammation, and oxidative stress, thereby delaying the aging process[83,84]. Additionally, the SIRT1 pathway has been implicated in protecting against age-related cognitive decline, renal aging, and vascular aging[85,86]. The modulation of SIRT1 pathways presents a promising therapeutic target for combating aging-related conditions.

With the ability of GSCRE and C2 to inhibit melanoma cells and demonstrate anti-aging properties, we have identified a potential therapeutic or supplementary compound that can both impede melanoma cell growth and offer anti-aging benefits. Figure 8 illustrates these properties, detailing how targeting specific proteins can achieve these effects.

We conducted cytotoxicity testing to assess the safety profile of GSCRE. The LD_{50} values of the extract were evaluated on melanoma cells and normal skin cells, alongside their respective controls. The findings indicated that the LD_{50} value of Caulersin (C2) demonstrated comparable levels of toxicity to Trametinib in melanoma cells, while exhibiting a greater tolerance for toxicity in normal cells compared to Trametinib. In comparison to Dabrafenib, C2 showed markedly higher levels of toxicity towards melanoma cells, while still maintaining a higher threshold for toxicity in normal cells. Therefore, C2 exhibits a considerable degree of safety, positioning it as a promising candidate for future alternatives in chemotherapy.

Our research has conducted a thorough investigation and successfully identified GSCRE compounds that exhibit anti-aging and anti-melanoma activities. This outcome was achieved through focused computational molecular docking followed by in vitro validation in a laboratory setting. By identifying compounds in GSCRE and understanding their biomolecular mechanisms, we can enhance our knowledge of potential agents for anti-aging and cancer treatment, thus establishing valuable resources for future research, specifically in the domain of cancers, particularly melanoma. However, it is crucial to expand and advance this research to subsequent stages. Conducting in vivo experiments on animals and clinical trials is essential to further evaluate the efficacy and safety of GSCRE and its compounds. Additionally, it is important to isolate each identified compound in GSCRE that demonstrates anti-aging and anti-cancer properties through computational analysis. Advancing the

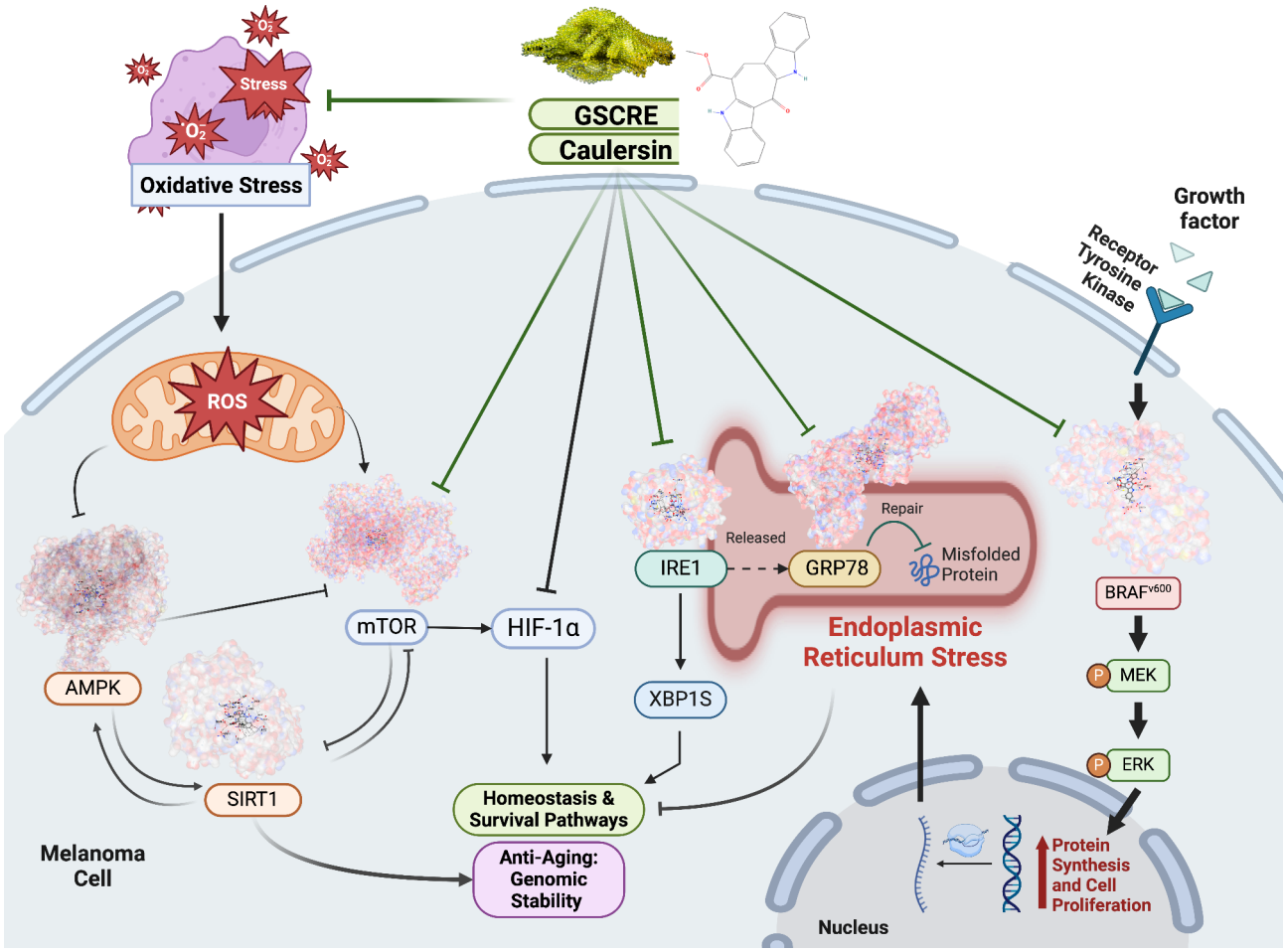

Fig. 8. Biomechanism of anti-aging and anti-melanoma via modulation of mTOR/AMPK/SIRT1 and GRP78/IRE1/BRAF by GSCRE.

development of these products individually and assessing their effectiveness through in vivo experimentation and subsequent clinical trials is essential.

Materials and methods

The profiling for active compunds in green seaweed *Caulerpa racemosa* extract (GSCRE)

The sample collection was carried out with official permission from the local authorities and the owner of the green seaweed pond. The green seaweed, *Caulerpa racemosa*, was sourced from a cultivation pond in Jepara Regency, located in the Central Java Province of Indonesia. The precise coordinates of the location are latitude 6°35'12.500" south and longitude 110°38'36.000" east. Botanical identification and authentication were verified by a knowledgeable biologist and the authors, following the guidelines of the National Center for Biotechnology Information (NCBI) Taxonomy ID 76317 (Eukaryota/Viridiplantae/Chlorophyta/Ulvophyceae/Bryopsidales/Caulerpaceae/Caulerpa). Specimens were collected for future documentation.

The methodologies employed in this investigation adhered strictly to the pertinent guidelines and regulations for in vitro and algae research. The authors state and confirm that the local authorities have approved sample collection and comply with relevant national and 'IUCN Policy Statement on Research Involving Species at Risk of Extinction Guidelines (all methods carried out in this study are in line or by applicable guidelines and regulations of in vitro and plant study). The sample utilized in this study was obtained from previous researchers[87]. The green seaweed was subjected to a meticulous cleansing procedure to remove any traces of soil particles. Subsequently, the material was securely wrapped and subjected to desiccation in a Memmert Incubator IN55 oven, maintained at a constant temperature of 60°C, for a duration of 72 hours. The dehydrated seaweed was sliced into minuscule fragments and pulverized into simplicia powder using a blender.

The simplicia powder was subsequently extracted utilizing the maceration technique. To macerate, 1,000 g of simplicia powder was immersed in 2 L of 96% ethanol for 72 h, with periodic stirring and filtering. The filtrate was concentrated using a rotary evaporator and then evaporated in an oven at 40 °C to obtain a concentrated extract. The extraction procedure was iterated thrice, and the resultant extract was preserved at a temperature of 10 °C (Fig. 9).

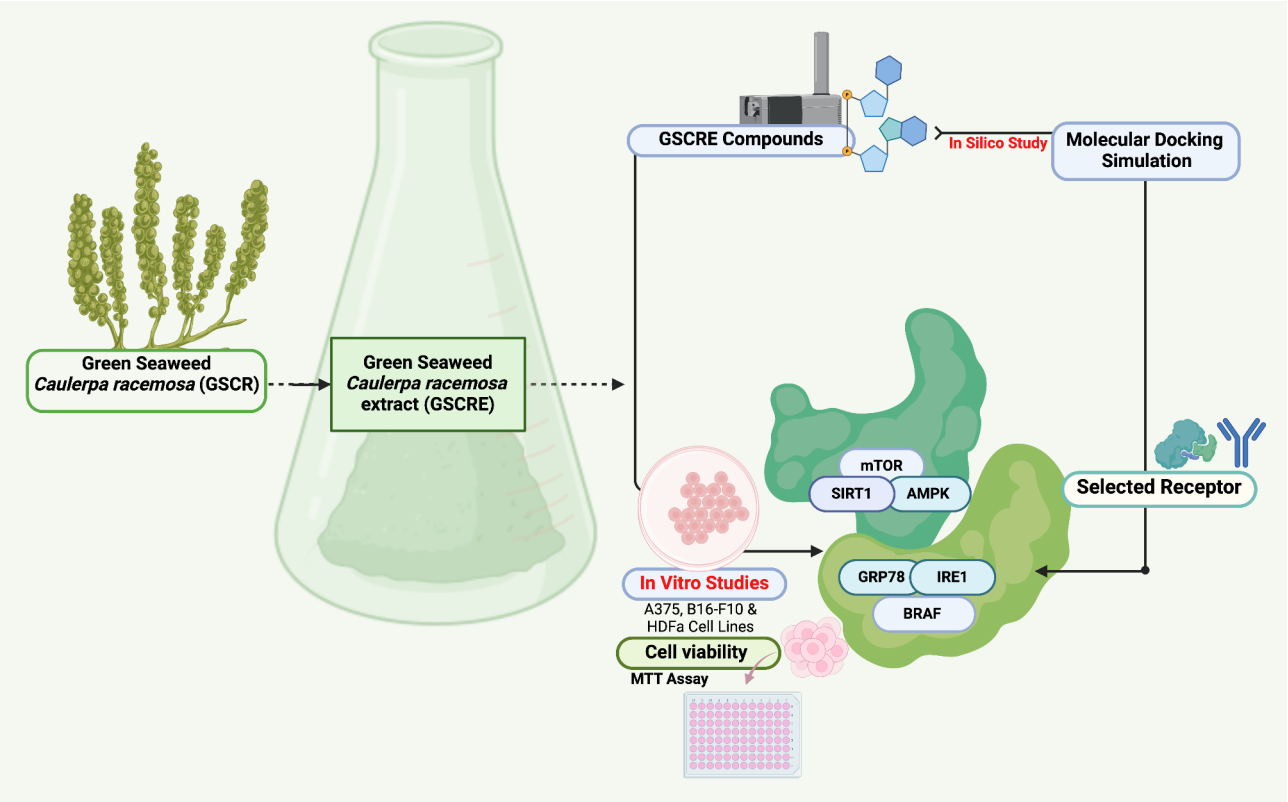

Fig. 9. Methodical schematic of GSCRE study flow.

An untargeted metabolomics analysis was conducted on extracts of green seaweed using both maceration and Soxhlet techniques. The analysis was performed utilizing Liquid Chromatography High-Resolution Mass Spectrometry (LC-HRMS) at the Faculty of Medicine, Brawijaya University, located in Malang, Indonesia. For the analysis, 50 µl of each extract were mixed with ethanol to reach a final volume of 1500 µl. Subsequently, the mixture was thoroughly agitated and strained prior to its introduction into the LC-HRMS. The LC-HRMS system employed a Thermo Scientific Dionex Ultimate 3000 RSLC nano HPLC system, which was outfitted with specialized solvents and columns. Furthermore, a Thermo Scientific Q Exactive mass spectrometer was utilized for high-resolution full scans and data-dependent MS/MS analysis. This comprehensive procedure guaranteed the accurate identification of metabolite profiles from the extracts. The methodologies employed in this study are derived from prior investigations carried out by Nurkolis et al.[88,89]. One limitation of our study is that we have not yet isolated each observed compound. In vitro testing will utilize commercially available compounds.

Evaluation of in silico study

Predicting the activities of bioactive compounds, analyzing toxicity, and assessing drug-likeness

The bioactivity of the compounds derived from *C. racemosa* was evaluated using the WAY2DRUG PASS prediction tool (https://www.way2drug.com/PassOnline/predict.php, accessed on July 11, 2024). This tool was utilized to assess the compounds' capacity to specifically target malignant melanoma tumors. The analysis involved conducting a Structure-Activity Relationship (SAR) analysis to compare the input compounds with established bioactive compounds. The Pa value, representing the probability of activity, is a prediction score given by the online tool that indicates the compound's potency[90]. A Pa value greater than 0.4 suggests potential bioactivity, such as anticancer properties, because it closely resembles known compounds in the database. Higher Pa values indicate more precise predictions. This study specifically examined compounds with Pa values greater than 0.4. Additionally, toxicity and drug-likeness analyses were performed to assess the pharmacokinetic characteristics and possible negative impacts of the compounds. The drug similarity characteristics of each ligand were assessed using Lipinski's Rule of Five (Ro5). The analyses were conducted using the Protox II database (https://tox-new.charite.de/protox_II/index.php?site=compound_input, accessed on July 11, 2024) and the ADMETLab 2.0 database (https://admetmesh.scbdd.com/service/evaluation/index, accessed on July 11, 2024). The SMILES notation for each compound was utilized as input for these analyses. The SMILES representations were acquired from PubChem (https://pubchem.ncbi.nlm.nih.gov, accessed on July 11, 2024), along with the corresponding data found in Supplementary Data Table S2.

Simulated molecular docking

The docking simulation was performed using CB-Dock2, an upgraded version of the CB-Dock server. CB-Dock2 utilizes cavity-detection-guided blind docking for protein-ligand interactions. This methodology

combines the processes of cavity identification, docking, and homologous template fitting, as described in previous publications[91]. CB-Dock2 streamlines the docking procedure by identifying binding sites, computing their coordinates and dimensions, adapting the size of the docking box based on the ligands under investigation, and executing molecular docking. The CurPocket method employs curvature-based cavity detection to forecast the binding sites of target proteins, while CB-Dock2 determines the binding positions of query ligands. For a thorough methodology, consult the designated publication[91]. The receptors with the highest centrality, connected to their respective signaling pathways, were chosen for additional analysis in molecular docking. The genetic material or proteins utilized were mTOR (PDB ID: 4JSV), AMPK (PDB ID: 6B1U), SIRT1 (PDB ID: 4I5I), GRP78 (PDB ID: 5F1X), IRE1 (PDB ID: 6W3K), and BRAF (PDB ID: 3OGJ).

Prior to docking, the CB-Dock2 server autonomously eliminated water molecules and other heteroatoms from the protein structures. All proteins served as receptors or targets for the ligand to bind to. The protein structures in .pdb format were obtained from the RSCB Protein Data Bank (https://www.rcsb.org; accessed on July 6, 2024). The ligands were acquired from PubChem in .sdf format (https://pubchem.ncbi.nlm.nih.gov; accessed on July 7, 2024). CB-Dock2 improves the accuracy of docking by combining cavity detection, docking, and homologous template docking. This integration enables the anticipation of binding sites and their affinities, which is advantageous for drug discovery. The affinity (ΔG) value is utilized to evaluate the efficacy of the ligand or target compound and to compare it with a control or standard drug.

Molecular dynamics simulations

Molecular dynamics (MD) simulations began with the retrieval of protein structures from the RCSB Protein Data Bank (www.rcsb.org). The proteins used in this study were BRAF (PDB ID: 3OGJ)[92], and mTOR (PDB ID: 4JSV)[93]. Refinement of the protein structure was carried out before simulation using Swiss PDB Viewer[94]. Protein topologies were generated using the pdb2gmx tool with the AMBER99SB-ILDN force field[95], while Caulersin topologies were prepared using ACPYPE[96]. The system was neutralized by adding NaCl under physiological pH conditions, and periodic boundary conditions (PBC) were applied. Long-range electrostatics were handled using the Particle-Mesh Ewald (PME) method, with Fast Fourier Transform (FFT) used for computational efficiency. The TIP3P water model was utilized to solvate the system. Following system setup, energy minimization was performed to remove steric clashes and stabilize the system. Equilibration was conducted in two phases: first, in the canonical ensemble (NVT) to stabilize the temperature, followed by the isothermal-isobaric ensemble (NPT) to stabilize pressure. The production phase also employed the NPT ensemble, maintaining a constant temperature of 310 K. The total simulation time was 100 nanoseconds, and all simulations were performed using GROMACS version 2022.2 [97]. Free energy calculations were performed for all frames using the molecular mechanics-generalized born surface area (MM-GBSA) approach, implemented through the UNI-GBSA[98], and gmx_MMPBSA software[99], Providing insights.

In vitro study on melanoma cell lines

The Faculty of Medicine, Universitas Brawijaya in Malang, Indonesia provided and cultured cell lines for melanoma cells with a BRAF mutation (A375, Sigma-Aldrich®, Darmstadt, Germany, catalog no. CB_88113005), melanoma cells with wild-type BRAF (B16-F10, ATCC®, Manassas, VA, USA, catalog no. CRL-6475), and normal skin cell lines (HDFa, ATCC®, catalog no. PCS-201-012). The A375, B16-F10, and HDFa cells (1×10^5) were cultured in 96-well plates using Dulbecco's Modified Eagle Medium (DMEM) supplemented with 10% Fetal Bovine Serum and 1% antibiotics (100 IU/mL Penicillin and 100 µg/mL Streptomycin), following the instructions provided by the manufacturer. After the cultured cells reached a confluence level of 80%, they were incubated at a temperature of 37 °C with a carbon dioxide concentration of 5%. Cells were regularly harvested using a trypsin-ethylenediaminetetraacetic acid (EDTA) solution from Thermo-Fisher Scientific, USA.

Assessment of the antiproliferative activity and cytotoxicity of GSCRE using the MTT assay

The cytotoxicity test was performed using the MTT method, following the protocols described by Nurkolis et al. and Lau et al.[17,88]. A375 melanoma cells with BRAF mutation, B16-F10 melanoma cells with wild-type BRAF, and HDFa normal dermal cell lines were cultivated on 96-well plates and subjected to a 24-hour incubation period. The cells were exposed to GSCRE and C2 at concentrations ranging from 0 to 175 µg/mL. The positive controls, Dabrafenib and Trametinib, were acquired from Sigma-Aldrich (Darmstadt, Germany) and underwent identical treatment as outlined in prior research. After the cells were treated, GSCRE, C2, Dabrafenib, and Trametinib were added to the cells and left to incubate for 24 h. Following incubation, the cells were rinsed with a 1X PBS solution and subsequently exposed to 100 µL of MTT solution at a concentration of 0.5 mg/mL. This incubation took place at 37 °C for a duration of 30 min. Afterward, 100 µL of DMEM stopper reagent was added to each well. The measurement of absorbance was conducted using a microplate reader, specifically at a wavelength of 550 nm. In order to mitigate potential bias, three sets of triple trials were carried out for each treatment group. The percentage of viable cells was determined using the following formula:

$$Percentage\ of\ Living\ Cells\ (\%) = \frac{A - B}{C - B}$$

Description = A: The absorbance of cell with treatment; B: The absorbance of blank samples; C: The absorbance of control cell.

The substances were classified based on the results of acute toxicity evaluation, using their median lethal dose (LD_{50}). The classification categories are as follows: extremely toxic (LD_{50} less than 5 mg/kg), highly toxic (LD_{50} between 5 and 50 µg/mL), moderately toxic (LD_{50} between 50 and 500 µg/mL), slightly toxic (LD_{50} between 500

and 5,000 µg/mL), practically non-toxic (LD50 between 5,000 and 15,000 µg/mL), and relatively harmless (LD_{50} greater than 15,000 µg/mL)[100].

mTOR/AMP/SIRT1 pathways and GRP78/IRE1/BRAF pathway protein expression

The in vitro analysis of the mTOR/AMPK/SIRT1 pathways and GRP78/IRE1/BRAF gene expressions was performed following the manufacturer's protocols. The reagents used included: Elabscience® Human mTOR (Mammalian Target of Rapamycin) ELISA Kit; Elabscience® AMPK alpha1/2 Polyclonal Antibody; Elabscience® Human SIRT1 (Sirtuin 1) ELISA Kit; Elabscience® Human GRP78 (Glucose Regulated Protein 78) ELISA Kit; ThermoFisher Scientific® IRE1 alpha Antibodies; Elabscience® BRAF Polyclonal Antibody Kit. To identify mTOR, AMPK, SIRT1, GRP78, IRE1, and BRAF, polyvinylidene difluoride membranes were treated with a blocking solution containing 5% skimmed dry milk in Tris-buffered saline with Tween (T-TBS) to inhibit non-specific binding of detection reagents. The buffer solution consisted of 0.1% Tween 20, 20 mmol/L Tris-HCl, 0.138 mol/L sodium chloride (NaCl; Sigma-Aldrich, Darmstadt, Germany), with a pH of 7.4. For detecting phosphorylated proteins, a blocking solution containing 5% bovine serum albumin (BSA) in T-TBS was used.

The methodology involved exposing the cell membranes to primary antibodies, followed by the utilization of secondary antibodies that were linked with peroxidase. The primary and secondary antibodies were diluted in a solution consisting of 5% BSA in T-TBS. The study aimed to examine the expression levels of mTOR, AMPK, SIRT1, GRP78, IRE1, and BRAF using an antibody-based technique. This method guaranteed accurate antibody dilution and appropriate incubation conditions. The experimental procedure began by adding 5000 A375 cells to each well, using 100 µL per well. After incubating for 24 h, the cells were treated with GSCRE at a concentration of 18 mM. The collected data were analyzed to determine the percentage value compared to the control group, which consisted of cells that either did not receive any treatment or were exposed to 0 mM GSCRE. The percentage value was determined using spectrophotometers (SmartSpec Plus from Bio-Rad Laboratories, Inc., Hercules, CA, USA) to measure optical density (OD) at wavelengths of 665 and 620 nm.

Data management and analysis

The statistical analysis utilized GraphPad Prism Premium 10 software for MacBook (GraphPad Software, Inc., San Diego, CA, USA) and SPSS 27.0 for Windows operating system. The Shapiro-Wilk test was utilized to evaluate the normality of data distributions. If the data exhibited a normal distribution with a p-value greater than 0.05, a One-Way ANOVA was employed to compare the means between the treatment groups. If the data did not satisfy the assumption of normality ($p < 0.05$), the Kruskal-Wallis test was utilized. Furthermore, the LD_{50}, which represents the median lethal concentration for melanoma cells, was established. The LD_{50} for cancer cells were analyzed using GraphPad non-linear regression package [log(inhibitor) vs. normalized response—variable slope].

Conclusions

This comprehensive study, integrating molecular docking simulations and ex vivo cellular studies, has identified novel molecules from green seaweed *Caulerpa racemosa* extract (GSCRE) with potential in combating human melanoma and aging. Caulersin (C2), a derivative of GSCRE, demonstrated significant activity in both the mTOR/AMP/SIRT1 and GRP78/IRE1/BRAF signaling pathways through in silico molecular docking and ex vivo cellular studies on the human A375 melanoma cell line with the BRAF-V600E mutation. The findings suggest that GSCRE, particularly C2 or Caulersin, holds promise for development as novel functional food ingredients aimed at combating aging and melanoma. However, further in vivo studies and clinical trials are necessary to confirm these results and fully establish their efficacy and safety.

Patents

The extraction method resulting from the work reported in this article has been registered as a patent by Fahrul Nurkolis in Indonesia.

Data availability

The data presented in this study are available on request from the corresponding author.

Received: 6 August 2024; Accepted: 31 October 2024
Published online: 11 November 2024

References

1. Laikova, K. V. et al. Advances in the understanding of skin cancer: Ultraviolet radiation, mutations, and antisense oligonucleotides as anticancer drugs. *Molecules* **24**, (2019).
2. Urban, K., Mehrmal, S., Uppal, P., Giesey, R. L. & Delost, G. R. The global burden of skin cancer: A longitudinal analysis from the global burden of disease study, 1990–2017. *JAAD Int.* **2**, 98–108 (2021).
3. The American Cancer Society medical and editorial content team. Melanoma skin cancer statistics. *Am. Cancer Soc.* (2024). https://www.cancer.org/cancer/types/melanoma-skin-cancer/about/key-statistics.html
4. Natarelli, N. et al. A review of current and pipeline drugs for treatment of melanoma. *Pharmaceuticals* 17, (2024).
5. Adeleke, S. et al. Melanoma-the therapeutic considerations in the clinical practice. *Ann. Palliat. Med.* **12**, 1355–1372 (2023).
6. Davis, L. E., Shalin, S. C. & Tackett, A. J. Current state of melanoma diagnosis and treatment. *Cancer Biol. Ther.* **20**, 1366–1379 (2019).
7. Mishra, H. et al. Melanoma treatment: From conventional to nanotechnology. *J. Cancer Res. Clin. Oncol.* **144**, 2283–2302 (2018).
8. Fathima, F. et al. Saraca Asoca: From traditional herb to modern drug as a cure for various diseases. *Curr. Drug Ther.* **18**, 285–297 (2023).

9. Husain, S. A. et al. A review on Valeriana Wallichii: Chemical composition and pharmacological research. *Curr. Tradit Med.* **9**, (2023).
10. Ahmed, N. et al. Comprehensive exploration of marine algae diversity, bioactive compounds, health benefits, regulatory issues, and food and drug applications. *Measurement: Food*. **14**, 100163 (2024).
11. Karthikeyan, A., Joseph, A. & Nair, B. G. Promising bioactive compounds from the marine environment and their potential effects on various diseases. *J. Genet. Eng. Biotechnol.* **20**, 14 (2022).
12. Menaa, F. et al. Marine algae-derived bioactive compounds: A new wave of nanodrugs? *Mar. Drugs* **19**, (2021).
13. Sharma, R., Mondal, A. S. & Trivedi, N. Anticancer potential of algae-derived metabolites: Recent updates and breakthroughs. *Future J. Pharm. Sci.* **9**, 1–44 (2023).
14. Permatasari, H. K. et al. Anti-cancer properties of Caulerpa racemosa by altering expression of Bcl-2, BAX, cleaved caspase 3 and apoptosis in HeLa cancer cell culture. *Front. Oncol.* **12**, 964816 (2022).
15. Mehra, R., Bhushan, S., Bast, F. & Singh, S. Marine Macroalga Caulerpa: Role of its metabolites in modulating cancer signaling. *Mol. Biol. Rep.* **46**, 3545–3555 (2019).
16. Nurkolis, F. et al. New Insight on in Vitro Biological activities of Sulfated Polysaccharides from Ulvophyte Green Algae. *Molecules* **28**, (2023).
17. Lau, V. et al. Green seaweed Caulerpa racemosa as a novel non-small cell lung cancer inhibitor in overcoming tyrosine kinase inhibitor resistance: An analysis employing network pharmacology, molecular docking, and in vitro research. *Mar. Drugs*. **22**, 272 (2024).
18. Susilowati, A., Mulyawan, A. E. & Putri, T. W. Antioxidant activity of the sea grape (Caulerpa Racemasa) as a lotion. *Orient. J. Chem.* https://doi.org/10.13005/ojc/350427 (2019).
19. Machado Urvanegia, A. C. et al. Reflectance confocal microscopy features of BRAF V600E mutated thin melanomas detected by immunohistochemistry. *PLoS One*. https://doi.org/10.1371/journal.pone.0179745 (2017).
20. Lee, S. H. et al. Genetic alterations among Korean Melanoma patients showing tumor heterogeneity: A comparison between primary tumors and corresponding metastatic lesions. *Cancer Res. Treat.* https://doi.org/10.4143/crt.2017.535 (2018).
21. Wu, X. et al. Mutations in BRAF codons 594 and 596 predict good prognosis in Melanoma. *Oncol. Lett.* https://doi.org/10.3892/ol.2017.6608 (2017).
22. Zhou, S. et al. Defining the criteria for reflex testing for BRAF mutations in cutaneous melanoma patients. *Cancers*. https://doi.org/10.3390/cancers13092282 (2021).
23. Dolinšek, T., Prosen, L., Čemažar, M., Potočnik, T. & Serša, G. Electrochemotherapy with bleomycin is effective in BRAF mutated melanoma cells and interacts with BRAF inhibitors. *Radiol. Oncol.* https://doi.org/10.1515/raon-2016-0042 (2016).
24. Popescu, A., Haidar, A. & Anghel, R. Treating malignant Melanoma when a rare BRAF V600M mutation is present: Case report and literature review. *Rom J. Intern. Med.* https://doi.org/10.1515/rjim-2017-0044 (2018).
25. Meevassana, J. et al. BRAF V600E immunohistochemistry predicts prognosis of patients with cutaneous melanoma in Thai Population. *Plast. Reconstr. Surg. Global Open*. https://doi.org/10.1097/gox.0000000000004605 (2022).
26. Ito, T. et al. Immunohistochemical BRAF V600E expression and Intratumor BRAF V600E heterogeneity in Acral Melanoma: Implication in melanoma-specific survival. *J. Clin. Med. Res.* https://doi.org/10.3390/jcm9030690 (2020).
27. Okuma, T. et al. Successful treatment of BRAF/MEK inhibitor-resistant advanced cutaneous melanoma with nivolumab plus ipilimumab combination therapy followed by intensity-modulated radiotherapy. *J. Dermatol.* https://doi.org/10.1111/1346-8138.15962 (2021).
28. Inozume, T. et al. Acquisition of resistance to vemurafenib leads to Interleukin-10 production through an aberrant activation of akt in a melanoma cell line. *J. Dermatol.* https://doi.org/10.1111/1346-8138.14651 (2018).
29. Jiang, C. C. et al. Data from inhibition of MEK sensitizes human melanoma cells to endoplasmic reticulum stress-Induced apoptosis. (2023). https://doi.org/10.1158/0008-5472.c.6496238.v1
30. Akinyemi, A. O. Unveiling the dark side of glucose-regulated protein 78 (GRP78) in cancers and other human pathology: A systematic review. *Mol. Med.* https://doi.org/10.1186/s10020-023-00706-6 (2023).
31. Chen, R., Niu, L., Wu, L., Liu, G. & Hong, K. Identification of an endoplasmic reticulum stress-associated gene signature to predict the immune status and prognosis of Cutaneous Melanoma. *Medicine*. https://doi.org/10.1097/md.0000000000030280 (2022).
32. Huang, Y. et al. Ovostatin 2 Knockdown significantly inhibits the growth, migration, and tumorigenicity of cutaneous malignant melanoma cells. *PLoS One*. https://doi.org/10.1371/journal.pone.0195610 (2018).
33. Casas, C. GRP78 at the centre of the stage in cancer and neuroprotection. *Front. Neurosci.* https://doi.org/10.3389/fnins.2017.00177 (2017).
34. Wang, C. et al. Estrogen receptor antagonist Fulvestrant inhibits proliferation and promotes apoptosis of Prolactinoma cells by regulating the IRE1/XBP1 signaling pathway. *Mol. Med. Rep.* https://doi.org/10.3892/mmr.2018.9379 (2018).
35. Mielczarek-Lewandowska, A., Sztiller-Sikorska, M., Osrodek, M., Czyż, M. & Hartman, M. L. 17-Aminogeldanamycin selectively diminishes IRE1α-XBP1s pathway activity and cooperatively induces apoptosis with MEK1/2 and BRAFV600E inhibitors in Melanoma cells of different genetic subtypes. *Apoptosis*. https://doi.org/10.1007/s10495-019-01542-y (2019).
36. Niessner, H. et al. BRAF inhibitors amplify the proapoptotic activity of MEK inhibitors by inducing ER stress in NRAS-Mutant melanoma. *Clin. Cancer Res.* https://doi.org/10.1158/1078-0432.ccr-17-0098 (2017).
37. Shen, K., Johnson, D. W., Vesey, D. A., McGuckin, M. A. & Gobé, G. C. Role of the unfolded protein response in determining the fate of tumor cells and the promise of multi-targeted therapies. *Cell. Stress Chaperones*. https://doi.org/10.1007/s12192-017-0844-3 (2018).
38. Eigner, K. et al. The unfolded protein response impacts Melanoma progression by enhancing FGF expression and can be antagonized by a chemical chaperone. *Sci. Rep.* https://doi.org/10.1038/s41598-017-17888-9 (2017).
39. Qing, B. Crosstalk between endoplasmic reticulum stress and multidrug-resistant cancers: Hope or frustration. *Front. Pharmacol.* https://doi.org/10.3389/fphar.2023.1273987 (2023).
40. Kumari, N., Reabroi, S. & North, B. J. Unraveling the molecular nexus between GPCRs, ERS, and EMT. *Mediators Inflamm.* https://doi.org/10.1155/2021/6655417 (2021).
41. Madden, E. C., Logue, S. E., Healy, S., Manié, S. N. & Samali, A. The role of the unfolded protein response in cancer progression: From oncogenesis to chemoresistance. *Biol. Cell.* https://doi.org/10.1111/boc.201800050 (2018).
42. Yang, Y. Endoplasmic reticulum stress and the unfolded protein response: Emerging regulators in progression of traumatic brain Injury. *Cell. Death Dis.* https://doi.org/10.1038/s41419-024-06515-x (2024).
43. Shi, R., Liao, C. & Zhang, Q. Hypoxia-driven effects in cancer: Characterization, mechanisms, and therapeutic implications. *Cells*. https://doi.org/10.3390/cells10030678 (2021).
44. Sykes, E., Mactier, S. & Christopherson, R. I. Melanoma and the unfolded protein response. *Cancers* doi: (2016). https://doi.org/10.3390/cancers8030030
45. Marelli, M. M. et al. Vitamin E Δ-Tocotrienol triggers endoplasmic reticulum stress-mediated apoptosis in human melanoma cells. *Sci. Rep.* https://doi.org/10.1038/srep30502 (2016).
46. Ojha, R. & Amaravadi, R. K. Targeting the unfolded protein response in cancer. *Pharmacol. Res.* https://doi.org/10.1016/j.phrs.2017.04.003 (2017).
47. Yoo, Y. S., Han, H. G. & Jeon, Y. J. Unfolded protein response of the endoplasmic reticlunogenicity. *Oxid. Med. Cell. Longev.* https://doi.org/10.1155/2017/2969271 (2017).

48. Belkacemi, L., Belalia, M., Djendara, A. C. & Bouhadda, Y. Antioxidant and antibacterial activities and identification of Bioactive compounds of various extracts of Caulerpa Racemosa from Algerian Coast. *Asian Pac. J. Trop. Biomed.* https://doi.org/10.4103/2221-1691.275423 (2020).
49. Sihono, S., Tarman, K., Madduppa, H. & Januar, H. I. Metabolite profiles and antioxidant activity of Caulerpa Racemosa with different handlings. *Squalen Bull. Mar. Fisheries Postharvest Biotechnol.* https://doi.org/10.15578/squalen.v13i3.355 (2018).
50. Shanura Fernando, I. P. et al. Squalene isolated from marine macroalgae Caulerpa Racemosa and its potent antioxidant and anti-inflammatory activities. *J. Food Biochem.* https://doi.org/10.1111/jfbc.12628 (2018).
51. Gurgel Rodrigues, J. A., Barros Benevides, N. M., Tovar, A. & de Mourão, P. A. ≪b> in vitro inactivation of thrombin generation by polysulfated fractions isolated from the tropical Coenocytic Green Seaweed ≪i> Caulerpa Racemosa (Caulerpaceae, Bryopsidales). *Acta Scientiarum Biol. Sci.* https://doi.org/10.4025/actascibiolsci.v39i3.32095 (2017).
52. Chumphoochai, K. Anti-obesity effects of marine macroalgae extract Caulerpa Lentillifera in a Caenorhabditis Elegans model. *Mar. Drugs*. https://doi.org/10.3390/md21110577 (2023).
53. Permatasari, H. K. et al. Metabolomic Assay, computational screening, and pharmacological evaluation of Caulerpa Racemosa as an anti-obesity with anti-aging by altering lipid profile and peroxisome proliferator-activated Receptor-Γ coactivator 1-A levels. *Front. Nutr.* https://doi.org/10.3389/fnut.2022.939073 (2022).
54. Dhanki, A., Sindhav, S. & Jadeja, B. A. Evaluation of the antimicrobial and antioxidant activity of two chlorophyceae and two rhodophyceae seaweeds from Porbandar coast. *Eur. J. Med. Plants*. https://doi.org/10.9734/ejmp/2020/v31i1630328 (2020).
55. CorrÃaa Alves, R. C. et al. Antimicrobial activity of seaweeds of Pernambuco, Northeastern Coast of Brazil. *Afr. J. Microbiol. Res.* https://doi.org/10.5897/ajmr2015.7616 (2016).
56. Tassakka, A. C. Green Algae Caulerpa Racemosa Compounds as antiviral candidates for SARS-CoV-2: In silico study. *Narra J.* https://doi.org/10.52225/narra.v3i2.179 (2023).
57. Hayes, C. et al. Coffee silverskin phytocompounds as a novel anti-aging functional food: A pharmacoinformatic approach combined with in vitro study. *Molecules*. **28**, 7037 (2023).
58. Daneshgar, N., Rabinovitch, P. S. & Dai, D. F. TOR signaling pathway in cardiac aging and heart failure. *Biomolecules*. https://doi.org/10.3390/biom11020168 (2021).
59. Bjedov, I. & Rallis, C. The target of rapamycin signalling pathway in ageing and lifespan regulation. *Genes*. https://doi.org/10.3390/genes11091043 (2020).
60. Ferrara-Romeo, I. et al. The mTOR pathway is necessary for survival of mice with short telomeres. *Nat. Commun*. https://doi.org/10.1038/s41467-020-14962-1 (2020).
61. Blagosklonny, M. V. Cell senescence, rapamycin and hyperfunction theory of aging. *Cell. Cycle*. https://doi.org/10.1080/15384101.2022.2054636 (2022).
62. Blagosklonny, M. V. & Anti-Aging Senolytics or gerostatics (unconventional view). *Oncotarget*. https://doi.org/10.18632/oncotarget.28049 (2021).
63. Han, X. et al. AMPK activation protects cells from oxidative stress-induced senescence via autophagic flux restoration and intracellular NAD(+) elevation. *Aging Cell.* **15**, 416–427 (2016).
64. Salminen, A., Kauppinen, A. & Kaarniranta, K. AMPK activation inhibits the functions of myeloid-derived suppressor cells (MDSC): impact on cancer and aging. *J. Mol. Med.* **97**, 1049–1064 (2019).
65. Salminen, A. AMPK signaling inhibits the differentiation of myofibroblasts: Impact on age-related tissue fibrosis and degeneration. *Biogerontology*. **25**, 83–106 (2024).
66. Gong, H. et al. miR-146a impedes the anti-aging effect of AMPK via NAMPT suppression and NAD+/SIRT inactivation. *Signal. Transduct. Target. Ther.* **7**, 66 (2022).
67. Yu, M. et al. Key Signaling pathways in aging and potential interventions for healthy aging. *Cells* 10, (2021).
68. Ryu, J. Y., Choi, H. M., Yang, H. I. & Kim, K. S. Dysregulated autophagy mediates sarcopenic obesity and its complications via AMPK and PGC1α Signaling pathways: potential involvement of Gut Dysbiosis as a pathological link. *Int. J. Mol. Sci.* **21**, (2020).
69. Yang, L., Shi, J., Wang, X., Zhang, R. & Curcumin Alleviates, D. Galactose-induced cardiomyocyte senescence by promoting autophagy via the SIRT1/AMPK/mTOR Pathway. *Evid. Based. Complement. Alternat. Med.* 2990843 (2022). (2022).
70. Cui, Z. et al. Therapeutic application of quercetin in aging-related diseases: SIRT1 as a potential mechanism. *Front. Immunol.* https://doi.org/10.3389/fimmu.2022.943321 (2022).
71. Yu, Y. et al. Oxidative stress impairs the Nur77-Sirt1 Axis resulting in a decline in organism homeostasis during aging. *Aging Cell.* https://doi.org/10.1111/acel.13812 (2023).
72. Kou, X. et al. Ampelopsin Attenuates Brain Aging of D-Gal-Induced Rats Through miR-34a-mediated SIRT1/mTOR Signal Pathway. *Oncotarget* (2016). https://doi.org/10.18632/oncotarget.12811
73. Fu, X. et al. The role of Procyanidins in delaying the premature ovarian insufficiency through Regulatory Sirt1-P53-P21 signaling pathway in female germline stem cells. (2023). https://doi.org/10.21203/rs.3.rs-2756953/v1
74. de Leite, P. L. et al. Higher Sirt1 is associated with a better body composition in master sprinters and untrained peers. *EJSS* (2022). https://doi.org/10.1080/17461391.2022.2138556
75. Nopparat, C., Sinjanakhom, P., Govitrapong, P. & Melatonin Reverses H2O2-induced senescence in SH-SY5Y cells by enhancing Autophagy via Sirtuin 1 Deacetylation of the RelA/p65 subunit of NF-κB. *J. Pineal Res.* https://doi.org/10.1111/jpi.12407 (2017).
76. Yan, J., Wang, J., He, J. C. & Zhong, Y. Sirtuin 1 in chronic kidney disease and therapeutic potential of targeting sirtuin 1. *Front. Endocrinol.* https://doi.org/10.3389/fendo.2022.917773 (2022).
77. Su, H., Gao, D., Chen, Y. & Zuo, Z. The relationship between Klotho and SIRT1 expression in renal aging related disease. *Int. J. Gen. Med.* https://doi.org/10.2147/ijgm.s384119 (2022).
78. Gao, Y. H. & Muscle, P. S. N. Gene combined with exercise contribute to healthy aging of skeletal muscle and lifespan by adaptively regulating Sirt1/PGC-1α and arm pathway. *PLoS One*. https://doi.org/10.1371/journal.pone.0300787 (2024).
79. Xu, C. et al. SIRT1 is downregulated by autophagy in senescence and ageing. *Nat. Cell. Biol.* https://doi.org/10.1038/s41556-020-00579-5 (2020).
80. Batiha, G. E., Al-Kuraishy, H. M., Al-Gareeb, A. I. & Elekhnawy, E. SIRT1 pathway in Parkinson's Disease: A faraway snapshot but so close. *Inflammopharmacology*. https://doi.org/10.1007/s10787-022-01125-5 (2022).
81. Liu, S. Pyrroloquinoline Quinone promotes human mesenchymal stem cell-derived Mitochondria to improve premature ovarian insufficiency in mice through the SIRT1/ATM/p53 pathway. *Stem Cell. Res. Ther.* https://doi.org/10.1186/s13287-024-03705-4 (2024).
82. Yin, J. et al. Gut microbiota-derived indole derivatives alleviate neurodegeneration in aging through activating GPR30/AMPK/SIRT1 pathway. *Mol. Nutr. Food Res.* https://doi.org/10.1002/mnfr.202200739 (2023).
83. Zhang, Z. et al. Study on the mechanism of radix astragali against renal aging based on network pharmacology. *Evid. Based Complement. Alternat Med.* https://doi.org/10.1155/2022/6987677 (2022).
84. Protective Action of SIRT1 activator aptamer in human skin cell line. JPTCP. (2023). https://doi.org/10.47750/jptcp.2023.30.05.035
85. Myers, M. J., Shaik, F., Shaik, F. & Mohamed, J. S. Skeletal muscle gene expression profile in response to caloric restriction and aging: A Role for SirT1. *Genes* doi: (2021). https://doi.org/10.3390/genes12050691
86. Kwon, S. H., Choi, H. G., Kang, Y. A. & Park, K. Depigmenting effect of Resveratrol is dependent on FOXO3a activation without SIRT1 activation. *Int. J. Mol. Sci.* https://doi.org/10.3390/ijms18061213 (2017).
87. Nurkolis, F., Permatasari, H. K. & LC-HRMS DATA OF Caulerpa racemosa8. doi: (2022). https://doi.org/10.6084/m9.figshare.20518485.v1

88. Nurkolis, F. et al. Ulvophyte Green Algae Caulerpa lentillifera: Metabolites profile and antioxidant, anticancer, anti-obesity, and in vitro cytotoxicity properties. *Molecules* **28**, (2023).
89. Nurkolis, F. et al. Dietary supplementation of Caulerpa racemosa Ameliorates cardiometabolic syndrome via regulation of PRMT-1/DDAH/ADMA pathway and gut microbiome in mice. *Nutrients* 15, (2023).
90. Daina, A., Michielin, O. & Zoete, V. SwissTargetPrediction: Updated data and new features for efficient prediction of protein targets of small molecules. *Nucleic Acids Res.* **47**, W357–W364 (2019).
91. Liu, Y. & Cao, Y. Protein-ligand blind docking using CB-Dock2. *Methods Mol. Biol.* **2714**, 113–125 (2024).
92. Kim, J. J. et al. Co-crystal structures of PKG Iβ (92–227) with cGMP and cAMP reveal the molecular details of cyclic-nucleotide binding. *PLoS One*. **6**, e18413 (2011).
93. Yang, H. et al. mTOR kinase structure, mechanism and regulation. *Nature*. **497**, 217–223 (2013).
94. Johansson, M. U., Zoete, V., Michielin, O. & Guex, N. Defining and searching for structural motifs using DeepView/Swiss-PdbViewer. *BMC Bioinform.* **13**, 173 (2012).
95. Lindorff-Larsen, K. et al. Improved side-chain torsion potentials for the Amber ff99SB protein force field. *Proteins*. **78**, 1950–1958 (2010).
96. Sousa da Silva, A. W. & Vranken, W. F. ACPYPE - AnteChamber PYthon Parser interfacE. *BMC Res. Notes*. **5**, 367 (2012).
97. Van Der Spoel, D. et al. GROMACS: Fast, flexible, and free. *J. Comput. Chem.* **26**, 1701–1718 (2005).
98. Yang, M. et al. Uni-GBSA: An open-source and web-based automatic workflow to perform MM/GB(PB)SA calculations for virtual screening. *Brief. Bioinform* **24**, (2023).
99. Valdés-Tresanco, M. S., Valdés-Tresanco, M. E., Valiente, P. A., Moreno, E. & Gmx_MMPBSA: A new tool to perform end-state free energy calculations with GROMACS. *J. Chem. Theory Comput.* **17**, 6281–6291 (2021).
100. Wallace Hayes, A. & Loomis, T. A. *Loomis's Essentials of Toxicology* (Elsevier, 1996).

Acknowledgements
Not applicable.

Author contributions
Conceptualization, D.W., B.K. and F.N.; methodology, D.W., F.N., R.A.S., B.K. and T.E.T.; software, F.N., P.P.P. and V.L.; validation, B.K., T.E.T., R.R.T. and N.A.T.; formal analysis, F.N., R.A.S., P.P.P. and D.W.; investigation, F.N., D.W. and V.L.; resources, F.N.; data curation, V.L., F.N., A.I.A. and D.W.; writing—original draft preparation, F.N., V.L., D.W., R.R.T., A.I.A. and B.K.; writing—review and editing, F.N., A.T., P.P.P., N.A.T., R.R.T., D.W., R.A.S., T.E.T., S.M. and B.K.; visualization, F.N. and V.L.; supervision, F.N., A.T., N.A.T., B.K., T.E.T. and R.R.T.; project administration, D.W. and F.N. All authors have read and agreed to the published version of the manuscript.

Funding
No Funding for this study/article.

Declarations

Competing interests
The authors declare no competing interests.

Informed consent
Not applicable.

Additional information
Supplementary Information The online version contains supplementary material available at https://doi.org/10.1038/s41598-024-78464-6.

Correspondence and requests for materials should be addressed to F.N.

Reprints and permissions information is available at www.nature.com/reprints.

Publisher's note Springer Nature remains neutral with regard to jurisdictional claims in published maps and institutional affiliations.